

String percolation and the first LHC data

I. Bautista^{1,2}, J. Dias de Deus² and C. Pajares¹

¹*Dpto. Física de Partículas and
Instituto galego de Física de Altas Enerxías
Universidade de Santiago de Compostela
Santiago de Compostela 15782
Galice, Spain*

²*CENTRA, Departamento de Física,
IST, Av Rovisco Pais,
1049-001 Lisboa, Portugal.*

E-mail: irais@fpaxp1.usc.es; jorge.dias.de.deus@ist.utl.pt; pajares@fpaxp1.usc.es

The results of string percolation on multiplicities and elliptic flow in AA and pp collisions are compared with LHC data showing a good agreement. We discuss the rapidity long range correlations and its relation to the height and longitudinal extension of the ridge structure. Finally we show that the dependence of the shear viscosity over entropy density ratio on the temperature, presents a minimum close to the critical temperature remaining small in the range of the RHIC and LHC energies.

1 String percolation

The percolation of strings [1][2][3] have described successfully the basic facts, obtained at RHIC and LHC, of the Physics of QCD matter at higher energy.

Strings are supposed to describe confined QCD interactions in an effective way. They carry color charges at the ends and an extended color field between the charges. They emit particles by string breaking and pair creation. Projected in the impact parameter they look like disks of radius $r_0 \simeq 0.2$ fm and two-dimensional percolation theory can be applied. As the energy or the size of the projectile or target increases interaction between strings occurs due to the overlapping of the strings and the general result, due to the

$SU(3)$ random summation of color charges, is that there is a reduction in multiplicity, and an increase in the string tension of formed clusters which means an increase of $\langle p_T^2 \rangle$.

The relevant variable is the transverse string density η_t ,

$$\eta_t \equiv \frac{\pi r_0^2}{S} N^s \quad (1)$$

where N^s is the number of strings and S the overlapping area. For η_t larger than a critical value η_t^c a large cluster extends over the whole surface covering the fraction $1 - e^{-\eta_t}$ of the total area which at $\eta_t = \eta_t^c$ is approximately 2/3. For homogeneous surface $\eta_t^c \simeq 1.2$ and for more realistic profiles $\eta_t^c \simeq 1.5$ [4].

The basic formulae are, for particle density [2][3]

$$\frac{dn}{dy} = F(\eta_t) N^s \mu_1 \quad (2)$$

and for $\langle p_T^2 \rangle$

$$\langle p_T^2 \rangle = \frac{\langle p_T^2 \rangle_1}{F(\eta_t)} \quad (3)$$

where $F(\eta_t)$ is the color reduction factor

$$F(\eta_t) = \sqrt{\frac{1 - e^{-\eta_t}}{\eta_t}} \quad (4)$$

and μ_1 and $\langle p_T^2 \rangle_1$ are the multiplicity and mean p_T^2 produced by the fragmentation of a single string.

The multiplicity distribution can be obtained from the cluster size distribution which approximately is a gamma function and the multiplicity distribution of the cluster, which we assume Poisson like. In this way, we obtain the negative binomial distribution [5].

$$P(n, s) = \frac{\Gamma(n+k)}{\Gamma(n+1)\Gamma(k)} \frac{\gamma^k}{(1+\gamma)^{n+k}}, \quad \gamma = \frac{k}{\langle n \rangle}, \quad (5)$$

where $\langle n \rangle$ is given by (5) and k is identical to

$$\Re \equiv \frac{\langle n(n-1) \rangle - \langle n \rangle^2}{\langle n \rangle^2} = \frac{\langle N^2 \rangle - \langle N \rangle^2}{\langle N \rangle^2} = \frac{1}{k}, \quad (6)$$

where N is the number of effective color sources and \Re the normalized two particle correlation. Since, from (3) the size area of one effective cluster $\pi r_0^2 F(\eta_t)$, and the area

covered by strings is $(1 - e^{-\eta})\pi R^2 < N >$ is given by [6].

$$< N > = \frac{(1 - e^{-\eta_t})R^2}{F(\eta_t)r_0^2} = (1 - e^{-\eta_t})^{1/2} \sqrt{\eta_t} \left(\frac{R}{r_0}\right)^2 \quad (7)$$

Note that

$$< N > / N^s = F(\eta_t) , \quad < n > = < N > \mu_1 \quad (8)$$

We observe that in the low density limit, there is not overlapping of strings and the particle density is essentially Poisson and we have $k \rightarrow \infty$. In the large η_t limit, the N effective strings behave like a single string, with $< N^2 > \simeq < N >^2$ and therefore $k \rightarrow < N > \rightarrow \infty$. At intermediate densities, k has a minimum close to the critical η_t^c , k is given by [6].

$$k = \frac{< N >}{(1 - e^{-\eta_t})^{3/2}} = \sqrt{\eta_t} (1 - e^{-\eta_t})^{-1} \left(\frac{R}{r_0}\right)^2 \quad (9)$$

In the glasma picture of color glass condensate also is obtained a negative binomial distribution. In CGC the multiplicity is given by the number of color flux tube (strings), $Q_s^2 R_A^2$, times the number of gluons produced by one, which is proportional to $1/\alpha_s(Q_s)$. On the other hand, k is the number of flux tubes, $Q_s^2 R_A^2$, which in the limit of high density coincides with (9) having the same A and s dependencies.

Concerning the p_T distributions, assuming a gaussian decay of each cluster, whose width is given by (3) and taking into account the gamma function distribution as the cluster size distribution we obtain the following distribution [6][8-10]

$$\frac{dN}{dp_T^2 dy} = \frac{dN}{dy} \frac{k' - 1}{k'} \frac{F(\eta_t)}{< p_T^2 >_1} \left(1 + \frac{F(\eta_t)p_T^2}{k' < p_T^2 >_1}\right)^{-k'}. \quad (10)$$

This formula is not valid for high p_T because we have assumed a gaussian distribution for the decay of a cluster without any power behavior corresponding to hard emissions. In (10) the k' is a function of η_t which has a qualitative similar dependence that k (may differ in the range of integration). At low p_T , (10) behaves like $\exp(\frac{-p_T^2}{< p_T^2 >})$ and at moderate p_T has a power like behavior. The formula (10) is valid at all energies and centralities including pp collisions, and gives a right description of RHIC and LHC data, up to $p_T \simeq 5$ GeV/c.

Note that at low energy density (10) behaves like $\exp(-p_T^2 / < p_T^2 >_1)$. As the energy density increases, k' decreases and there is a departure of the exponential behavior. However above critical point k' increases again and it is recover the exponential behavior.

2 Multiplicity distributions

The new LHC data has shown that the multiplicity at central rapidity rise faster in central $Pb - Pb$ collisions than in pp collisions. On the other hand, the data show the dependence in the centrality of the multiplicity in AA is the same at LHC and RHIC energies. These two facts are explained in our approach.

The apparently different behavior of the multiplicities is due to energy conservation. In fact, in $Pb - Pb$ collisions the number of strings grows like the number of collisions, $N_A^{4/3}$, and the energy available only grows like A . Therefore, at not very high energy, there will be strings that can not be formed because there is not energy available. We take into account this effect assuming that the number of strings increases like $N_A^{1+\alpha(s)}$ where $\alpha(s)$ is 0 at low energy and goes to $1/3$ at very high energy. In this way we obtain [11].

$$\frac{1}{N_A} \frac{dn}{dy} |_{N_A N_A} = \frac{dn}{dy} |_{pp} \left[1 + \frac{F(\eta_{N_A}^t)}{F(\eta_p^t)} (N_A^{\alpha(s)} - 1) \right], \quad (11)$$

with

$$\eta_{N_A}^t = \eta_p^t N_A^\alpha \left(\frac{A}{N_A^{2/3}} \right), \quad \alpha = \frac{1}{3} \left(1 - \frac{1}{1 + \ln(\sqrt{s/s_0} + 1)} \right) \quad (12)$$

and

$$\frac{dn}{dy} |_{pp} = a \left(\frac{s}{m_p} \right)^{\lambda/2}. \quad (13)$$

In Fig. 1 we show our results for $\lambda = 0.23$ together with the data for AA and pp [12-14]. In Fig. 2, we show our results concerning the centrality dependence for Pb-Pb at LHC energy and Cu-Cu and Au-Au at RHIC energy.

Concerning the rapidity dependence, there is not limiting fragmentation scaling in the percolation approach [12] and the evolution with energy is very different for different values of the pseudorapidity η . This is clearly seen in Fig. 3 where is shown $\frac{dn}{d\eta} |_{ch}$ for different η values and their energy dependence. It is seen that for central pseudorapidity $\eta = 0$ the energy dependence is weaker, $s^{\lambda/2}$, than for high multiplicity $\eta \simeq 5$, that is s^λ [15].

3 Long range rapidity correlations and the ridge structure

The correlation introduced in formula (6) is relevant for the discussion of rapidity long range correlations and the ridge structure, first seen in Au-Au collisions and central Cu-Cu collisions at RHIC as well in high multiplicity pp and Pb-Pb collisions at LHC. In

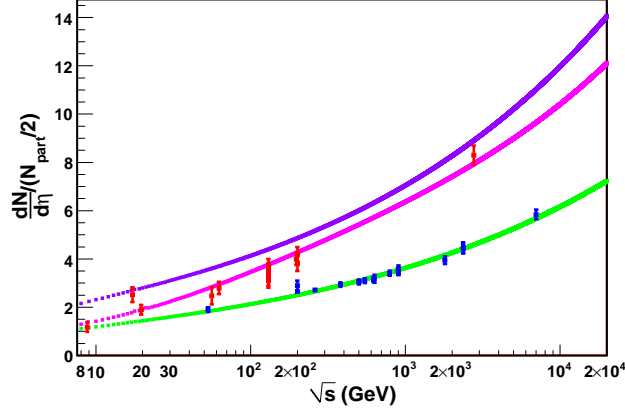


Figure 1: $dN_{ch}/d\eta$ from formula (11) at different \sqrt{s} , lines in pink, and green correspond to Au-Au and p-p collisions respectively. Line in purple shows the asymptotic result for (11) with $F(\eta^t) \rightarrow 1/\sqrt{\eta^t}$ and $\alpha \rightarrow 1/3$.

those collisions it was detected a correlated broad peak of particles extended in rapidity and localized in an azimuthal angle. The strength of the ridge structure is proportional to $\Re \frac{dn}{dy}$.

The ridge structure seen in high multiplicity pp events [16] was predicted [17][18] in the percolation approach, using equation (12) that indicates that the string density for high multiplicity events in pp at LHC is equivalent to the string density for Au-Au peripheral collisions a $Cu - Cu$ central collisions at $\sqrt{s} = 200$ GeV.

In percolation, we have from (2) and (6) [16]

$$\Re \frac{dn}{dy} = \frac{\langle N \rangle}{k} = (1 - e^{-\eta_t})^{3/2} \quad (14)$$

As the density and/or energy increases the height of the near side ridge structure increases slowly. Similar behavior is found in CGC [19] where

$$\Re \frac{dn}{dy} = \frac{1}{\alpha_s(Q_s)}. \quad (15)$$

The values of $\Re \frac{dn}{dy}$ are related to the value of the parameter b , which measures the rapidity

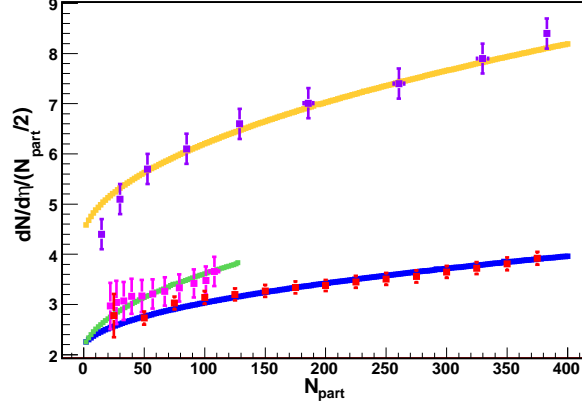


Figure 2: $dN_{ch}/d\eta$ from formula (11) at different centralities at 200 GeV. Lines in blue and green are the corresponding predictions for Au-Au and Cu-Cu. Points shown in red and pink are the corresponding data for Au-Au and Cu-Cu from reference at 200 GeV. Line in orange is the result of the formula (11) at 2.76 TeV compared with ALICE data in purple.

long range correlations and it is defined by

$$b = \frac{\langle n_F n_B \rangle - \langle n_F \rangle \langle n_B \rangle}{\langle n_F^2 \rangle - \langle n_F \rangle^2} \quad (16)$$

where n_F and n_B stand for the multiplicity in a forward and backward bins, separated by some rapidity gap to avoid short range correlations in the numerator of (17).

It is shown that [20][21]

$$b = \frac{1}{1 + \frac{k}{\langle N \rangle}}, \quad (17)$$

and therefore

$$b = \frac{1}{1 + \frac{1}{\Re \frac{dn}{dy}}} = \frac{1}{1 + (1 - e^{-\eta_t})^{-3/2}}. \quad (18)$$

At low energy density $b \rightarrow 0$, and at high density $b \rightarrow 1/2$. Similar behavior is obtained in CGC [22][23].

Notice that k plays an important role in determining the long range rapidity correlations and also controls the inverse of the width of the KNO distribution $\langle n \rangle / P_n$ as a

function of $n / \langle n \rangle$. As far as k grows with energy density above the critical percolation value we predict that the width should decrease above this value. For minimum bias pp collisions the critical value is reached close to $\sqrt{s} = 14$ TeV. The data on pp shows in the measured range (up to 7 TeV) k is decreasing [24].

4 Elliptic flow

In a precisely $b = 0$, in AA or pp collisions the projected area in the impact parameter plane is a circle populated by disks approximately in a azimuthal uniform way. If $b \neq 0$ we have a projected almond. If we imagine the projected almond to be obtained by a deformation of the circle, it is clear that the string density is larger along the smaller, x axis, than the density along the y axis. It is intrinsic anisotropy that determines the existence of elliptic flow v_2 . Also energy loss arguments support a sizable v_2 . Notice that in percolation we have in the initial state interactions of the partons of the individual strings as a consequence of the color arrangement which is produced inside the formed cluster. The fragmentation of this large cluster produces a thermal distribution of particles [30] and provide us the required early thermalization as far as the fragmentation time is around 1 fm.

In order to compute v_2 we introduce the transverse azimuthal density [26-28].

$$\eta_\phi^t = \eta^t \left(\frac{R}{R_\phi} \right)^2 \quad (19)$$

where

$$R_\phi = R_A \frac{\sin(\phi - \alpha)}{\sin\phi} \quad (20)$$

$$\alpha = \sin^{-1} \left(\frac{b}{2R_A} \sin\phi \right) \quad (21)$$

and

$$\frac{\pi R_A^2}{4} \simeq \frac{1}{2} \int_0^{\pi/2} d\phi dR_\phi^2 \quad (22)$$

Introducing (20) into the transverse momentum distribution (10) and expanding the resulting distribution in powers of $(R_\phi^2 - R^2)$, retaining the first two terms, we obtain

$$v_2(p_T^2, y) = \left[\frac{2}{\pi} \int_0^{\pi/2} d\phi \cos 2\phi \left(\frac{R_\phi}{R} \right)^2 \right] \left(\frac{e^{-\eta} - F(\eta^t)^2}{2F(\eta^t)} \right) \frac{F(\eta^t) p_T^2 / \langle p_T^2 \rangle_1}{(1 + F(\eta^t) p_T^2 / \langle p_T^2 \rangle_1)} \quad (23)$$

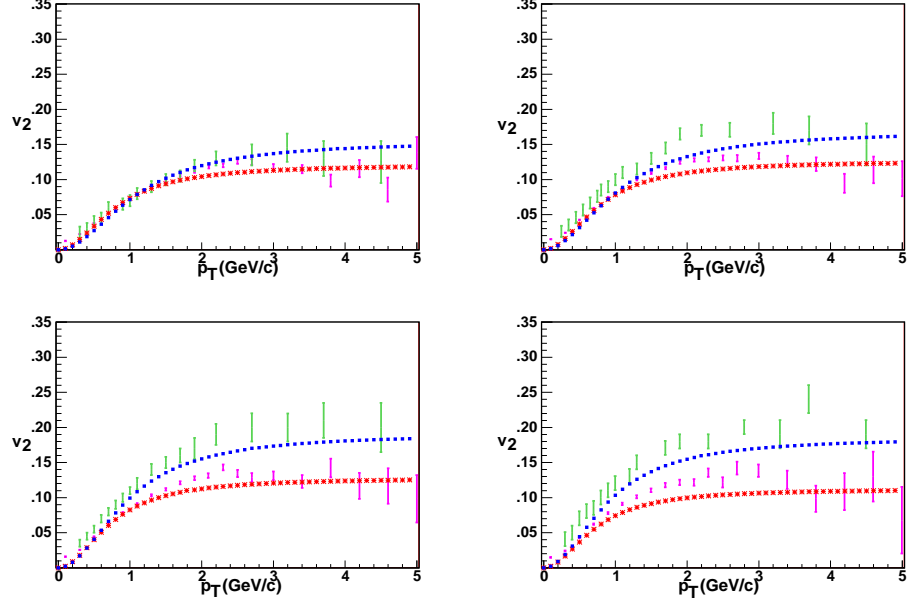


Figure 3: Color online stars in red and blue squares correspond to our predictions for $\sqrt{s} = 200$ GeV and $\sqrt{s} = 2.76$ TeV energies, and error-bars in green and pink are the respective data from RHIC and LHC for centralities 10 – 20% , 20 – 30% , 30 – 40% , 40 – 50%, figure caption order from top left to bottom right respectively.

We observe that at low p_T the dependence on η^t is given by $(e^{-\eta_t} - F^2(\eta_t))/2F(\eta^t)$ which remain approximately constant for the values of η^t corresponding to RHIC and LHC.

In Fig. 3 we compare our results on the dependence of v_2 on p_T with RHIC and LHC data at different centralities [12]-[29]. In Fig. 4 we compare the centrality dependence with ALICE experimental data [12]. In Fig. 5 we show our results for π , k , and p at $\sqrt{s} = 2.76$ TeV. We obtain a very good agreement with RHIC and LHC data, only our results on p are slightly different from data. Notice that our results are obtained from the close universal formula (24) valid for all energies and centralities. Apart from the parameter $\langle p_T^2 \rangle_1$ the only input is the string density η_t fixed from the multiplicity.

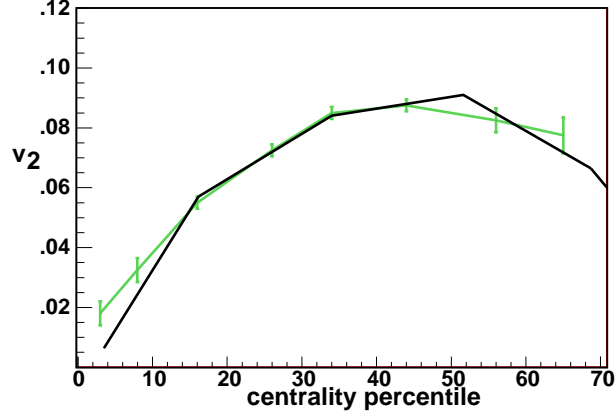


Figure 4: Integrated v_2 at $\sqrt{s} = 2.76$ TeV compared with ALICE data.

5 Shear viscosity entropy density ratio

The shear viscosity to entropy density ratio is a measured of the fluidity and the RHIC and LHC data show a low value, lower than most of the known substances. In string percolation we obtain also a low η/s [31]. In fact, in percolation the strong color field inside the large cluster produces de-acceleration which can be seen as a thermal temperature [30][32] by means of Hawking-Unruh effect. The temperature is given by

$$T(\eta^t) = \sqrt{\langle p_T^2 \rangle_1 / 2F(\eta^t)} \quad (24)$$

On the other hand, from the relativistic kinetic theory η/s is given by

$$\frac{\eta}{s} = \frac{T\lambda}{5} \quad \lambda = \frac{1}{n\sigma_{tr}} \quad (25)$$

where λ is the mean free path, n the number density and σ_{tr} the transport cross section.

From equation (7) we have

$$n = \frac{1 - e^{-\eta^t}}{\pi r_0^2 F(\eta^t) L} \quad (26)$$

and

$$\sigma_{tr} = S_1 F(\eta^t) = \frac{\pi r_0^2 \langle p_T^2 \rangle_1}{2T^2} \quad (27)$$

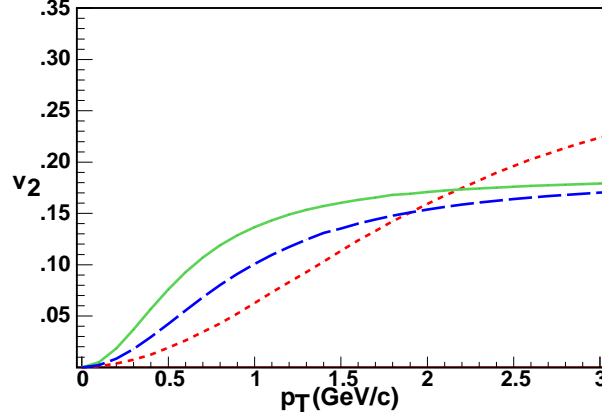


Figure 5: Color online red dotted line, green solid line and blue dashed line are correspond to the proton, kaon, and pion predictions for central $Pb - Pb$ collisions at $\sqrt{s} = 2.76$ TeV.

From (26) and (27) we obtain

$$\frac{\eta}{s} = \frac{L\sqrt{\langle p_T^2 \rangle_1 \eta_t^{1/4}}}{5\sqrt{2}(1 - e^{-\eta_t})^{5/4}} \quad (28)$$

In Fig. 6 we show η/s as a function of T/T_c . Close to the critical temperature presents a minimum and remains small in the RHIC and LHC range growing slowly.

Acknowledgements

We thank J. G. Milhano, A. S. Hirsch, R. P. Scharenberg and B. Srivastava who collaborates in part of the work reported here. We thank the support of the FCT/Portugal project PPCDT/FIS/5756682004, the project FPA2008-01177 of MICINN of Spain, the Consolider project and the conselleria Educacion da Xunta de Galicia.

References

- [1] N. Armesto, M. A. Braun, E. G. Ferreiro and C. Pajares, Phys. Rev. Lett. **77** (1996) 3736; M. Nardi and H. Satz, Phys. Lett. B **442** (1998) 14

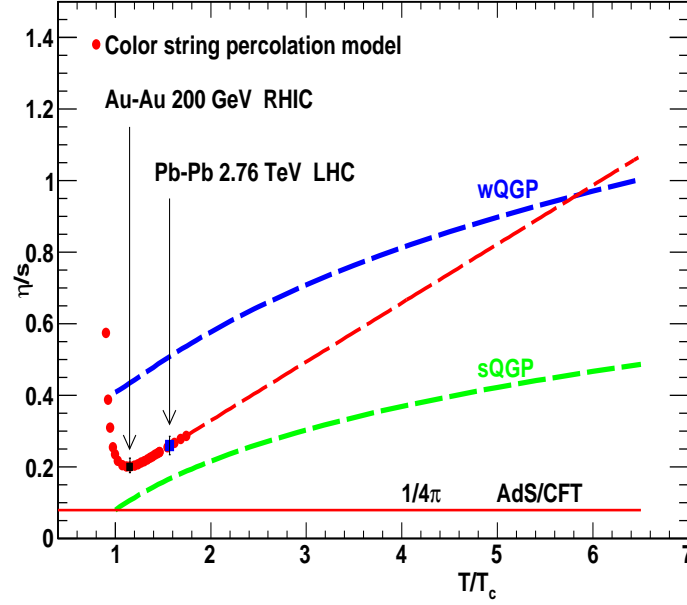


Figure 6:

- [2] M. A. Braun and C. Pajares, Phys. Rev. Lett. **85** (2000) 4864 [hep-ph/0007201].
M. A. Braun and C. Pajares, Eur. Phys. J. C **16** (2000) 349 [hep-ph/9907332].
- [3] M. A. Braun, F. Del Moral and C. Pajares, Phys. Rev. C **65** (2002) 024907 [hep-ph/0105263].
- [4] A. Rodrigues, R. Ugoccioni and J. Dias de Deus, Phys. Lett. B **458** (1999) 402 [hep-ph/9812364].
- [5] J. Dias de Deus, E. G. Ferreira, C. Pajares and R. Ugoccioni, Eur. Phys. J. C **40** (2005) 229 [hep-ph/0304068].
- [6] J. Dias de Deus and C. Pajares, Phys. Lett. B **695** (2011) 211
- [7] A. Dumitru, F. Gelis, L. McLerran and R. Venugopalan, Nucl. Phys. A **810** (2008)

- [8] L. Cunqueiro, J. Dias de Deus, E. G. Ferreira and C. Pajares, Eur. Phys. J. C **53** (2008) 585
- [9] C. Pajares, Eur. Phys. J. C **43** (2005) 9 [hep-ph/0501125].
- [10] J. Dias de Deus and R. Ugoccioni, Eur. Phys. J. C **43** (2005) 249.
- [11] I. Bautista, J. Dias de Deus, J. G. Milhano, C. Pajares to appear.
- [12] K. Aamodt *et al.* [The ALICE Collaboration], Phys. Rev. Lett. **105** (2010) 252302
- [13] P. Brogueira, J. Dias de Deus and C. Pajares, Phys. Rev. C **75** (2007) 054908 [hep-ph/0605148].
- [14] B. B. Back *et al.* [PHOBOS Collaboration], Phys. Rev. C **65** (2002) 061901 [nucl-ex/0201005].
- [15] I. Bautista, J. D. de Deus and C. Pajares, arXiv:1102.3837 [hep-ph].
- [16] V. Khachatryan *et al.* [CMS Collaboration], JHEP **1009** (2010) 091
- [17] P. Brogueira, J. Dias de Deus and C. Pajares, Phys. Lett. B **675** (2009) 308
- [18] L. Cunqueiro, J. Dias de Deus and C. Pajares, Eur. Phys. J. C **65** (2010) 423
- [19] S. Gavin, L. McLerran and G. Moschelli, Phys. Rev. C **79** (2009) 051902
- [20] M. A. Braun, C. Pajares and V. V. Vechernin, Phys. Lett. B **493** (2000) 54 [hep-ph/0007241].
- [21] P. Brogueira, J. Dias de Deus and C. Pajares, Phys. Lett. B **675** (2009) 308
- [22] N. Armesto, L. McLerran and C. Pajares, Nucl. Phys. A **781** (2007) 201 [hep-ph/0607345]. N. Armesto, M. A. Braun and C. Pajares, Phys. Rev. C **75** (2007) 054902 [hep-ph/0702216 [HEP-PH]].
- [23] F. Gelis, T. Lappi and L. McLerran, Nucl. Phys. A **828** (2009) 149
- [24] KAamodt *et al.* [ALICE Collaboration], Eur. Phys. J. C **65** (2010) 111
- [25] M. A. Braun and C. Pajares, Eur. Phys. J. C **71** (2011) 1549
- [26] I. Bautista, J. Dias de Deus and C. Pajares, Phys. Lett. B **693** (2010) 362
- [27] I. Bautista, L. Cunqueiro, J. D. de Deus and C. Pajares, J. Phys. GG **37** (2010) 015103

- [28] I. Bautista, J. D. de Deus and C. Pajares, arXiv:1102.3837 [hep-ph].
- [29] S. Manly *et al.* [PHOBOS Collaboration], Nucl. Phys. A **774** (2006) 523 [nucl-ex/0510031].
- [30] J. Dias de Deus and C. Pajares, Phys. Lett. B **642** (2006) 455 [hep-ph/0607101].
- [31] J. D. de Deus, A. S. Hirsch, C. Pajares, R. P. Scharenberg and B. K. Srivastava, arXiv:1106.4271 [nucl-ex].
- [32] D. Kharzeev, E. Levin and K. Tuchin, Phys. Rev. C **75** (2007) 044903 [hep-ph/0602063]. P. Castorina, D. Kharzeev and H. Satz, Eur. Phys. J. C **52** (2007) 187